Journal of Applied Fluid Mechanics, Vol. 11, No. 5, pp. 1421-1432, 2018.
Available online at www.jafmonline.net, ISSN 1735-3572, EISSN 1735-3645.
DOI: 10.29252/jafm.11.05.28847

Comparative Study of Reversal Flow during the Evaporation or Condensation of Water and Ethanol Film in a Vertical Channel

K. Sellami [1†], N. Labsi[1], M. Feddaoui[2], M. Oubella[2], Y. K Benkahla[1] and M. Najim[2]

[1] *Transfer Phenomena Laboratory, RSNE Team, FMGP, University of Science and Technology Houari Boumediene, BP. 32 El Alia, 16111 Bab Ezzouar, Algiers Algeria*
[2] *Laboratory of Energy, Materials and Systems Engineering, National School of Applied Sciences of Agadir, University of Ibn Zohr, Morocco*

†*Corresponding Author Email: sellami_karima@yahoo.fr*

(Received January 31, 2018; accepted April 4, 2018)

ABSTRACT

A comparative study of reversal flow is carried out to investigate the effect of thermal and mass buoyancy forces with evaporation or condensation along a vertical channel. The highlight is focused on the effects of phase change of two different liquid films having widely different properties, on heat and mass transfer rates in the channel. The evaporation occurs along isothermal and wetted walls. The induced laminar upward flow consists of a mixture of blowing air and vapour of water or ethanol. Various combinations of thermal and solutal boundary conditions (cooling and heating modes) are considered to investigate extensively their influence on the flow development. A two-dimensional steady state and elliptical flow model is used and the liquid film is assumed extremely thin. The governing equations of the model are solved by FVM and the velocity-pressure fields are treated with the SIMPLER algorithm. The results show that the buoyancy forces have a significant effect on the hydrodynamic, thermal and mass fields of both gas mixtures. In addition, the flow reversal is predicted with a relatively high temperature difference between the air-mixture and the wetted walls.

Keywords: Evaporation; Condensation; Cooling mode; Heating mode; Vertical channel; Buoyancy forces; Reversal flow; Elliptical flow model.

NOMENCLATURE

C_p	specific heat of the fluid at constant pressure
D_h	hydraulic diameter
D	mass diffusivity
f	friction factor
g	gravitational acceleration
H	channel width
h_M	mass transfer coefficient
Gr_M	Solutal Grashof number
Gr_T	Thermal Grashof number
Gr^+	Total Grashof number
h_{fg}	latent heat of vaporization
k	thermal conductivity
L	channel length
N	buoyancy ratio
P	pressure
Re	Reynolds number
Ri_M	Solutal Richardson number
Ri_T	Thermal Richardson number
Ri^+	Total Richardson number
T	temperature
U_0	gas inlet velocity
V	velocity
W	species mass fraction
x	longitudinal coordinate
y	transverse coordinate

Greek symbols

β_M	mass expansion coefficient
β_T	thermal expansion coefficient
ϕ_0	relative humidity of the air-vapour mixture.
μ	dynamic viscosity
ν	kinematic viscosity
ρ	density

Indices and exponents

m	average.
v	liquid vapour.
w	wall
0	inlet.

1. INTRODUCTION

The study of combined heat and mass transfer during in the evaporation of a pure fluid by convection flow in vertical parallel-plate channel has received considerable attention because of its wide range of applications, such as distillation, thermal protection of system components from a high temperature gas stream, cooling of electronic equipment and design of cooling towers. Due to such expanded applications, heat and mass transfer of air stream with liquid film evaporation has received considerable attention of researchers over the past decades.

Many studies were conducted with different geometric configurations and various thermal and solutal boundary conditions. Lin *et al.* (1988) analyzed numerically the combining effect of thermal and solutal buoyancy forces on laminar forced convection heat transfer in a vertical tube. The results show that the heat transfer processes involved in the flow is dominated by latent heat transport owing to the evaporation of the liquid film. They showed also, that at fixed wall temperature, the ratio of the latent heat flux to the sensible heat flux has a minimum value. Yan and Lin (1988) and Yan *et al.* (1989) investigated the influences of a wetted wall on laminar mixed convection heat transfer in vertical ducts. In their studies, the authors assumed that the liquid film was extremely thin on the wetted wall, so that it was considered as a boundary condition for heat and mass transfer only. Debbissi *et al.* (2003) studied numerically the evaporation of water by mixed and free convection in a vertical channel. The authors explain the existence of the inversion temperature by considering heat and mass transfer in the evaporation process. Huang *et al.* (2005) have conducted a numerical investigation of the enhancement of mixed convection heat transfer through film evaporation in a vertical duct. The study focuses on the influence of the film vaporization and condensation on the heat and mass transfer in ducts in the presence of constant temperature and concentration. The result of their study suggests that the heat transfer rate is enhanced by latent heat transport due to the evaporation or condensation of the liquid film.

The heat and mass transfer phenomenon by evaporation or condensation is encountered in many industrial applications, in heat exchangers, for refrigeration application where reversal flow problem is frequent. In fact, under given conditions, the evaporation process may generate high evaporative mass flow rate at the interface. In consequence, the very high concentration of vapour raises the buoyancy forces and the gas flow may change the direction and returns back to the inlet of the channel. Therefore, a non-uniform distribution of temperature and species results in the channel. This non-uniform distribution deteriorates the evaporator performances and reduces the system efficiency. All the above literature surveys show that the parabolic model cannot predict this phenomenon of reversal flow in vertical ducts in the presence of important Archimedes forces. Therefore, flow reversal with combining heat and mass transfer has received only limited attention. However, it was extensively studied in only thermal convection problems. The criteria of flow reversal was presented by Cheng *et al.* (1990) in an analytical study of the flow reversal phenomenon and heat transfer characteristics of developed laminar combined free and forced convection in a heated vertical channel. The effect of buoyancy and axial conduction on hydrodynamic and heat transfer characteristics has been systematically studied by Wang *et al.* (1994) in the inlet regions of horizontal and vertical pipes. The authors present also the numerical results for mixed convection. The regime of reverse flow is identified for both heating and cooling cases in both geometries. Desrayaud and Lauriat (2001) presented a numerical investigation of the flow reversal phenomenon for laminar mixed convection of air in a vertical parallel-plate channel of finite length. Their results show that the regime of reversed flow is identified for high values of the Peclet number. They also showed that the channel length has no influence on the occurrence of the reversal flow provided for a ratio of the length and the width channel higher than 10. Hammou *et al.* (2004) conducted a numerical study on the evaporation or condensation in mixed convection during the downward flow of moist air into a vertical channel with parallel walls. Their results show that the buoyancy forces affect significantly the axial velocity profiles, the friction factor, the sensible Nusselt number and the Sherwood number. Later, Cherif *et al.* (2011) presented an experimental investigation of the effect of film evaporation on mixed convective heat and mass transfer in a vertical rectangular channel.

As far as flow reversal in combined with heat and mass transfer is concerned, Salah El-Din (1992) presents an analytical study on the effect of thermal and mass buoyancy forces of fully developed laminar forced convection in a vertical channel. Criteria for the flow reversal occurrence has been presented. Azizi *et al.* (2007) investigated numerically the effects of thermal and solutal buoyancy forces on both upward and downward flows of air in a vertical parallel-plates channel; they also predict the flow reversal for an upward flow with a relatively high temperature difference between air and the walls. Oulaid *et al.* (2010) showed that buoyancy forces induce flow reversal for high air temperature and mass fraction at the channel entrance for an upward flow of warm humid air. The conditions for the existence of flow reversal have also been determined for different aspect ratios and mass diffusion Grashof numbers. The same authors (Oulaid *et al.* 2012) presented a numerical study of combined heat and mass transfer with phase change in an inclined channel. Their results show that the effects of the buoyancy forces on the hydrodynamic, thermal and mass fields are important; these effects depend on the channel inclination. A chart of flow reversal has been established for different inclination angles in their study. Kassim *et al.* (2011) analyzed the effect of inlet air humidity on an upward air flow in a

humidifier intended for a humidification-dehumidification desalination system. Their results show that the airflow is seriously affected by the humidity. They found that the flow reversal occurs near the isothermal plate and its magnitude is strongly depends on the air humidity at the entrance, and increases the vapour condensation. Recently, Oubella *et al.* (2015) evaluated the evaporation by mixed convection heat and mass transfer of three different liquid films evaporation in a vertical channel in combination with the isothermal and wetted walls. Their major results show that a small value of both the inlet gas temperature and the gas Reynolds number as well as a high volatility of the liquid film enhance the airflow cooling.

In the literature survey, the flow reversal with combining heat and mass transfer has not received much attention; the majority of the published work concerns the evaporation of water film with assuming a constant thermo-physics properties and adopting Boussinesq approximation whereas other liquids play an important role in practical applications with large variations in thermos-physical properties. This scope motivates the present study by analyzing the effects of the evaporation of two pure liquid films (water and ethanol), selected for their large difference in properties, on the heat and mass transfer rates in a vertical channel. On the other hand, various combinations of thermal and solutal boundary conditions for the two modes (cooling or heating) are considered to investigate extensively, using an elliptical flow model, their influence on the reversed flow with combination to mixed heat and mass transfer with phase change, and to determinate the conditions in which the reversal flow occurs. This will help to the design and improvement of cooling and air conditioning devices by avoiding the reversal flow.

2. PROBLEM FORMULATION

2.1 Physical Problem

The physical model studied in this paper consists of a vertical channel formed of two parallel plates of length L and a channel width H (Fig. 1). The vertical plates are wetted by a thin film of water or ethanol and maintained at a constant temperature T_w. The channel is traversed by a upward flow of humid air with a constant temperature T_0, a uniform relative humidity ϕ_0 and a uniform velocity U_0.

For the mathematical formulation of the problem, the following simplifying assumptions are taken into consideration:

- The flow is laminar and two dimensional,
- Humid air is an ideal gas mixture,
- Radiation, viscous dissipation, the work of the pressure forces and the Soret and Dufour effects are negligible,
- The effect of the superficial tension is negligible.

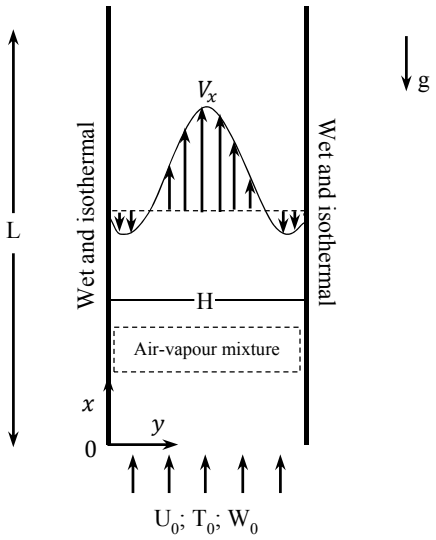

Fig. 1. Schematic view of the physical problem.

2.2 Governing Equations and Boundary Conditions

From the above assumptions, the bi-dimensional flow of the gas mixture is described in the (x,y) coordinate system and can be written as follow:

$$\frac{\partial(\rho_m V_x)}{\partial x}+\frac{\partial(\rho_m V_y)}{\partial y}=0 \tag{1}$$

$$\frac{\partial(\rho_m V_x^2)}{\partial x}+\frac{\partial(\rho_m V_x V_y)}{\partial y}= -\frac{\partial p}{\partial x}-\rho_m g+\frac{\partial}{\partial x}\left(\mu_m\frac{\partial V_x}{\partial x}\right)+\frac{\partial}{\partial y}\left(\mu_m\frac{\partial V_x}{\partial y}\right) \tag{2}$$

$$\frac{\partial(\rho_m V_y V_x)}{\partial x}+\frac{\partial(\rho_m V_y^2)}{\partial y}= -\frac{\partial p}{\partial y}+\frac{\partial}{\partial x}\left(\mu_m\frac{\partial V_y}{\partial x}\right)+\frac{\partial}{\partial y}\left(\mu_m\frac{\partial V_y}{\partial y}\right) \tag{3}$$

$$\frac{\partial(\rho_m V_x C_p T)}{\partial x}+\frac{\partial(\rho_m V_y C_p T)}{\partial y}=\frac{\partial}{\partial x}\left(k_m\frac{\partial T}{\partial x}\right)+\frac{\partial}{\partial y}\left(k_m\frac{\partial T}{\partial y}\right)+ \rho_m D_m\left(C_{pv}-C_{pa}\right)\left(\frac{\partial T}{\partial y}\frac{\partial W}{\partial y}\right) \tag{4}$$

$$\frac{\partial(\rho_m V_x W)}{\partial x}+\frac{\partial(\rho_m V_y W)}{\partial y}= \frac{\partial}{\partial x}\left(\rho_m D_m\frac{\partial W}{\partial x}\right)+\frac{\partial}{\partial y}\left(\rho_m D_m\frac{\partial W}{\partial y}\right) \tag{5}$$

The governing Eqs. (1-5) are subjected to the following boundary conditions:

- At the channel inlet ($x=0, 0<y<H$):

$$V_x=U_0,\ V_y=0,\ T=T_0 \text{ and } W=W_0 \tag{6}$$

According to the Dalton's law and the equation of state for ideal gas mixture, the inlet mass fraction of water vapor is calculated by the following expression:

$$W_0 = \frac{p_v(T_0)M_v}{p_v(T_0)M_v + (p - p_v(T_0))M_a} \quad (7)$$

Where M_v and M_a are the molecular weight of liquid vapour and air respectively, p is the thermodynamic pressure of gas mixture and $p_v(T_0)$ is defined as:

$$p_v(T_0) = \varphi_0 p_v^{sat}(T_0) \quad (8)$$

Where ϕ_0 is defined as relative humidity.

- At the walls ($y = 0$ and $y = H$, $0 < x < L$)

$$V_x = 0,\ V_y = V_e,\ T = T_w,\ W = W_w \quad (9)$$

The transverse velocity of the air-vapour mixture at the walls is given by:

$$V_e = -\frac{D_m}{1 - W_w}\frac{\partial W}{\partial y}\bigg|_w \quad (10)$$

- At the channel outlet ($0 < y < H$ and $x = L$):

$$\frac{\partial V_x}{\partial x} = V_y = \frac{\partial T}{\partial x} = \frac{\partial W}{\partial x} = 0 \quad (11)$$

One of the constraints to be satisfied is the overall mass balance for the two systems of mixture, defined as:

$$\int_0^H \rho V_x\, dy = \rho_0 U_0 H + \int_0^L \rho V_e\, dx \quad (12)$$

3. HEAT/MASS TRANSFER AND FLOW CHARACTERISTICS

In order to evaluate thermal, mass and hydrodynamic properties of the evaporation within the channel, a set of parameters are calculated.

The transfer of the energy between the channel wetted walls and the airflow with the presence of mass transfer depends in one hand on the fluid temperature gradient at the wetted walls resulting in a sensible heat transfer and on the rate of mass transfer resulting in a latent heat transfer in the other hand.

The local Nusselt number along the wall is defined as:

$$Nu_t = \frac{h\ D_h}{k} = \frac{q_t\ D_h}{k(T_w - T_m)} = Nu_s + Nu_l \quad (13)$$

Where h denote the local heat transfer coefficient, Nu_s and Nu_l are the local Nusselt numbers for sensible and latent heat transfer, respectively, and are evaluated by:

$$Nu_s = \frac{-2H}{T_w - T_m}\left(\frac{\partial T}{\partial y}\right)_{y=0} \quad (14)$$

$$Nu_l = \frac{-2H}{1 - W_w}\frac{\rho D_m h_{fg}}{k(T_w - T_m)}\left(\frac{\partial W}{\partial y}\right)_{y=0} \quad (15)$$

In a similar manner, the local Sherwood number on the wetted wall is given by:

$$Sh = \frac{h_M\ D_h}{D} = \frac{-2H}{(1 - W_w)(W_w - W_m)}\left(\frac{\partial W}{\partial y}\right)_{y=0} \quad (16)$$

The fanning friction factor is given by the following equation:

$$f = \frac{2}{\rho U_0^2}\mu\frac{\partial V_x}{\partial y}\bigg|_w \quad (17)$$

Solutal Grashof number

$$Gr_M = \frac{g\beta_M\ D_h^3(W_w - w_0)}{\nu^2} \quad (18)$$

Thermal Grashof number

$$Gr_T = \frac{g\beta_T\ D_h^3(T_w - T_0)}{\nu^2} \quad (19)$$

Reynolds number

$$\mathrm{Re} = \frac{\rho U\ D_h}{\mu} \quad (20)$$

Richardson number

$$Ri = \frac{Gr}{\mathrm{Re}^2} \quad (21)$$

In the present study, the thermo-physical properties of the gas mixtures are considered to be variable, depending on both temperature and concentration. They are calculated from the pure component data Perry (1999) by means of mixing rules (Reid 1977) applicable to any multi-component mixtures.

4. NUMERICAL MODELLING AND VALIDATION OF THE COMPUTER CODE

The system of elliptical equations governing the flow, heat and mass transfer as well as the associated boundary conditions are discretized by means of the finite volume method proposed by Patankar (1980). The velocity-pressure coupling is treated with the SIMPLER algorithm. The resulting set of discretized equations are reorganized into a tri-diagonal matrix equation and iteratively resolved using the TDMA algorithm. The convergence criterion of the numerical solution is based on the absolute normalized residuals of the equations that were summed for al cells in the computational domain. When the largest residual of all variables falls below 10^{-6} at all nodes of the grid the convergence is considered achieved.

4.1 Grid Independence Test

To check the grid independence, refinement tests were performed to an upward flow in a vertical channel with wet and isothermal walls kept at T_w = 20 °C, with an aspect ratio γ = 1/100. Several grid sizes are considered ranging from 150×40

to 250×60. The humid air flowing in the channel is under the following inlet conditions: T_0 = 30 °C, ϕ_0 = 10 % and Re_0 = 300. The results of this study are obtained by comparing the values of the average total sensible Nusselt number (Nu_s), average Sherwood number (Sh) and the friction factor (f_{Re}). It is clear from table 1 that the changes in these parameters with respect to the grid refinement are less than 0.5%. The grid size of 200×50 according to x and y directions respectively, is sufficient to acquire the results.

Table 1 Comparison of average total sensible Nusselt number, average Sherwood number and the friction factor for different grids.
(T_0 = 30 °C, ϕ_0 = 10 % and Re_0 = 300)

	$Nu_{s\_average}$	$Sh_{\_average}$	f_{Re} (x = 1m)
150×40	7.8472	7.9506	23.21
150×50	7.8495	7.9527	23.23
150×60	7.8512	7.9542	23.23
200×40	7.8462	7.9509	23.21
200×50	7.8507	7.9548	23.23
200×60	7.8526	7.9565	23.23
250×40	7.8504	7.9548	23.21
250×50	7.8528	7.9575	23.23
250×60	7.8545	7.9590	23.23

4.2 Comparison with Previous Studies

In order to guarantee the accuracy and validity of our in house code, we present comparisons with both experiment and numerical studies available in the literature. Our code has already been used for simulating many configurations; see for instance the paper of Feddaoui and his co-workers (Oubella *et al.*, 2015).

4.2.1 Experiment Film Evaporation on Mixed Convection

The comparison is done for the case of a vertical rectangular channel of aspect ratio ($\gamma = 1/10$). The two parallel channel walls are wetted by a water film and heated by a constant heat flux qw = 750 W m², while the other walls are dry and thermally insulated. An upward flow of humid air ($\phi_0 = 76.5\%$) enters the channel with a uniform velocity ($Re_0 = 1620$) and a constant temperature T_0 = 26.7 °C. The comparison between our results and the experimental study of Cherif *et al.* (2011) is presented in table 2. The corresponding numerical and experimental results of gas mixture temperature are satisfactory, with the exception of the case near the walls where the maximum relative gap in the gas mixture is about 6.7 % and that is located at the channel outlet.

4.2.2 Numerical Film Evaporation on Mixed Convection

The second comparison is done for the case of a mixed convection problem in a vertical channel. Dry air enters the channel with a uniform velocity profile (Re_0 = 300) and temperature (T_0 = 10 °C). The vertical walls are maintained at a constant temperature (T_w = 60 °C). The Grashof number is varied ($4.71\times10^4 \le Gr_T \le 1.27\times10^6$) by varying the width of the channel (0.02 m ≤ H ≤ 0.06 m).

Figure 2 presents the local Nusselt number along the non-dimensional axial length (x/D_h Pe) compared with the results of Desrayaud and Lauriat (2001). A very good agreement between both results is observed since the relative difference is less than 2%.

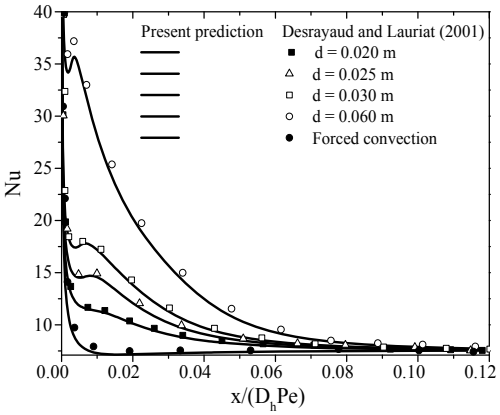

Fig. 2. Evolution of the sensible Nusselt number.

Table 2 Variation of temperature profiles along the channel

	Experiment data Cherif *et al.* (2011)	Present Prediction	Experiment data Cherif *et al.* (2011)	Present Prediction	Experiment data Cherif *et al.* (2011)	Present Prediction
y(m)	x = 0.05 m		x = 0.25 m		x = 0.5 m	
0.0000	48.00	50.02	48.90	50.02	50.01	50.02
0.0030	32.10	35.83	33.00	41.39	34.40	43.04
0.0115	28.10	26.71	29.00	27.81	29.90	29.43
0.0200	27.50	26.70	27.10	26.72	29.00	27.01
0.0300	27.60	26.70	27.70	26.73	28.90	27.02
0.0385	27.80	26.70	28.60	27.37	30.00	28.85
0.0470	32.20	26.70	33.10	39.21	33.90	44.07
0.0500	48.30	39.70	48.30	49.49	50.30	54.41

Table 3 Operating conditions and parameters of studied cases. (Re = 300)

Case	T_0 (°C)	ϕ_0 (%)	W_0 (10^{-2})	T_w (°C)	W_w (10^{-2})	Gr_T	Gr_M	Ri_T	Ri_M
	Water								
1	50	19.5	1.4492	20	1.4492	-200301.96	0.0	-2.67	0.000
2	50	50	3.8822	20	1.4492	-197081.94	-31351.10	-2.18	-0.340
3	20	50	0.7214	20	1.4492	0.0	12261.30	0.00	0.136
4	20	50	0.7214	50	7.9500	274225.6	117605.4	3.04	1.300
	Ethanol								
1	50	19.9	8.955	20	8.955	-240220.56	0.0	-3.18	0.000
2	50	50	21.40	20	8.955	-279792.51	139331.6	-3.10	1.540
3	20	50	4.550	20	8.955	0.0	-51380.90	0.00	-0.570
4	20	50	4.550	50	39.64	381046.61	-485543.0	4.23	-5.390

5. RESULTS AND DISCUSSION

In the present study, results were obtained for two stream gas mixtures: air-water and air-ethanol, flowing along a vertical channel of 0.02 m width and 1.5 m length. The air enters through the channel at a uniform upwind velocity U_0 (Re_0 = 300). In order to investigate the effect of wall and inlet conditions on the development of velocity profiles and the characteristics of heat and mass transfer, a range of each parameter is considered (table 3).

In light of practical situations, the selected combinations of T_0, T_w and ϕ_0 are specified in Table 3. The corresponding values of the two Grashof numbers and other relevant parameters are also indicated. Negative values of the Grashof number indicate that the corresponding buoyancy force acts in the direction of gravity and so, aids the entering downward flow or opposes the entering of upward flow.

In our cases, under the same operating conditions, many combinations are considered depending on the thermophysical properties of each fluid. Note that in cases 2 and 4, the thermal and solutal buoyancy forces act in the same direction for water film, whereas they act in opposing direction for ethanol film. Furthermore, in case 1, the thermal buoyancy acts solitary and opposing the flow for both fluids. On the other hand, the mass diffusion Grashof number is positive, zero or negative, depending on the absolute humidity of the entering air. In case 3, the solutal buoyancy force is therefore aiding the flow for water film and opposing it for ethanol film. For both systems, the case of forced convection $(Gr_T = Gr_M = 0)$ is also reported for comparison purposes.

Besides the Grashof numbers, the Richardson number Ri can be considered and it describes the relative intensity of the buoyancy force in comparison with the inertia force. The two Richardson numbers of consideration are the thermal Richardson Ri_T and the solutal Richardson number Ri_M.

For comparing the behaviour of the two studied fluids, it is of interest to plot the evolution of some thermophysical properties. The evolution of the saturated pressure of water and ethanol gas is presented in Fig. 3(a). It is clear that the saturated pressure of ethanol gas is higher than the water vapour. Consequently, the ethanol gas is more volatile than water vapour particularly for higher gas temperature. Figure 3(b) illustrates the effect of the temperature on latent heat of vaporisation for both gases. As disclosed from Fig. 3(b), water needs more energy to be evaporated than ethanol.

In order to evaluate the thermal and solutal buoyancy effects on the airflow, a number of computations were carried out for various combinations of mass fraction of moist air, inlet and wall temperatures (Table 3). The axial velocity profiles for water and ethanol vapours in upward flow for cooling and heating cases close to the channel entrance (x = 0.1 m) are depicted in Figs. 4 and 5, respectively. The case of forced convection is also reported for comparison.

In the cooling case (Fig. 4), we notice a distortion of the axial velocity profile for both vapours. The strong buoyancy forces are shown in case 1 for ethanol (Gr+ = -2.4×105) and water (Gr+ = -2×105) and in case 2 for water (Gr+ = -2.28×105). The net effect of these forces acts in the opposite direction of the upward flow (since Gr+ < 0, the combined buoyancy forces act in the downward direction) and decrease the flow near the channel walls. This decrease induces a reversal flow in this region. Therefore, axial velocity takes negative values. The decrease of the velocity close to the wetted walls is compensated by the intensification of the flow on the channel axis in order to satisfy the mass conservation. Moreover, this figure shows that the axial velocity profile is more distorted for high values of moist air temperature and humidity

at the entrance in cases of water, unlike the case 2 of ethanol when the solutal buoyancy act inversely to thermal buoyancy. In this later case, the solutal buoyancy force aids the upward flow and hence, reduces the distortion of the velocity profile. Additionally, in comparison with pure forced flow, evaporation produces a significant increase in axial velocity at the core region.

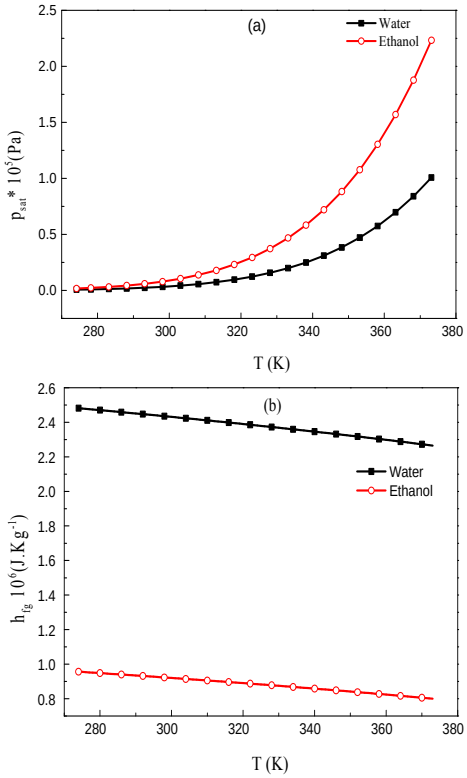

Fig. 3. Evolution of thermo-physicals properties of water and ethanol with temperature. (a) Saturated pressure (b) Latent heat of vaporization

It should be noted also that the intensity of the flow velocity of the air-water mixture is higher than that of the air-ethanol mixture. This is owing to the average density of air-ethanol mixture, which is higher compared with the air-water mixture. A careful analysis of Fig. 5 for the heating mode reveals that ethanol exhibits characteristics opposite to those observed in the case of the evaporation of water film. As in the case 4 of water film (Fig. 5(a)), the velocity profile is characterized by an acceleration of the flow near the walls and symmetrical concavity in channel centre, resulting in distortion to satisfy the mass conservation. This behaviour results of the strong aiding buoyancy forces that act in the direction of the upward flow ($Gr^+ = 3.9\times10^5$), contrary to the case of ethanol film where we notice a slight deceleration ($Gr^+ = -1\times10^5$) of the flow near the channel walls compensated by an acceleration of the flow in the centre region. This behaviour is the consequence of the values of the solutal Grashof number that are higher than those of the thermal Grashof number; the latter indicate that the dominant buoyancy force here is the solutal one.

Comparison between case 3 and 4 indicates that a rise in wall temperature causes an increase in the axial velocity, in accordance with the increase in the amplitude of the buoyancy forces through thermal and mass diffusion and a greater net quantity of liquid vapour evaporating into the air stream for a higher temperature. In case3, the solutal buoyancy act lonely and aides the flow of water film, whereas it opposes the flow for ethanol. The latter, explained readily the light distortion in velocity profile close to the walls for ethanol and non-distortion in velocity profile for water.

In order to visualize the development of airflow inside the channel in more detail, streamlines are shown in Fig. 6(a) for cooling mode, and Fig. 6(b) for heating mode for both vapour mixtures. These figures show that the streamlines are deflected near the entrance and close to the walls; this deflection is caused by the transverse gradients of temperature and mass fraction, which are significant in this region.

The inspection of case 2 (cooling mode) of Fig. 6(a) shows the appearance of recirculation cells near the walls. These cells indicate negative values of the axial velocity owing to reversal flow in this zone. While in the centre, an acceleration of the flow is noticed in order to satisfy the mass conservation unlike to case 4 (heating mode), where the temperature of the wall is higher than the mist air at the inlet for the water film. We notice also that the flow accelerates near the hot walls and decelerates in the channel centre as already explained (Fig. 5(a)). The cells centred close to the channel center correspond to minimal upward velocities near the channel entrance. This behaviour can be explained by the fact that the water density decreases as the flow moves forward into the channel, while it increases for ethanol. This is due to the low evaporation rate of the water film (W_w = 0.0795) against that of ethanol (W_w = 0.3964), which provide a strong solutal buoyancy forces near the wetted walls. In addition, the volatility of the water film is the lowest compared to ethanol, as previously shown in Fig. 3(a).

However, as the air mixture moves downstream, the temperature and the mass fraction gradients decrease. Thus, the effect of the buoyancy forces vanishes, the velocity profile recovers, and the streamlines are nearly parallel and attains its asymptotic fully developed parabolic profile.

Figure 7 represents the isotherms in both cooling (a) and heating (b) modes for the two mixtures systems. The effects of reversal flow at the walls are clearly seen near the channel entrance through the isotherms. By analysing the isotherms, it is found that the temperature distribution in the center part of the channel entrance tends to take constant values. In the cooling mode, the evolution of the temperature profiles of both air-water and air-ethanol mixtures has the same tendencies. These figures show that the air cools down due to the heat transfer toward the wetted walls and therefore, to mass transfer due to the film condensation of vapours. However, careful

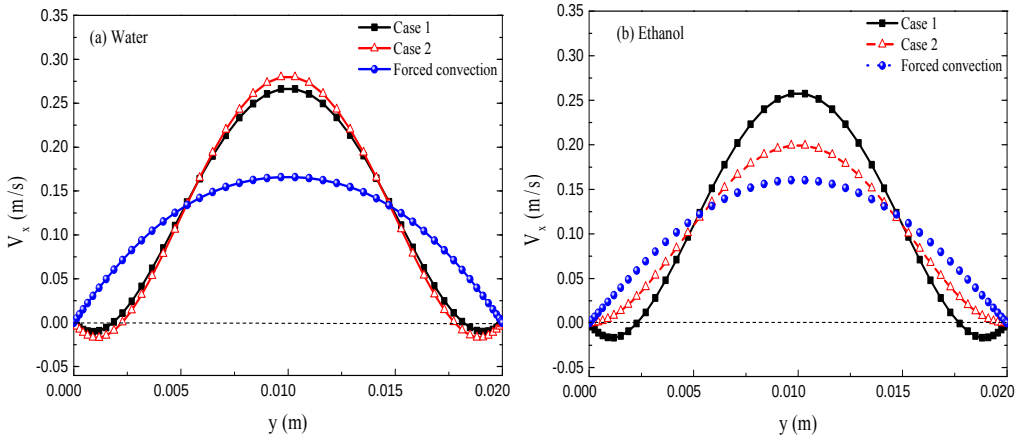

Fig. 4. Axial velocity profiles of water (a) and ethanol (b) at x = 0.1 m. Re_0 = 300, T_0 = 50 °C, T_w = 20°C.

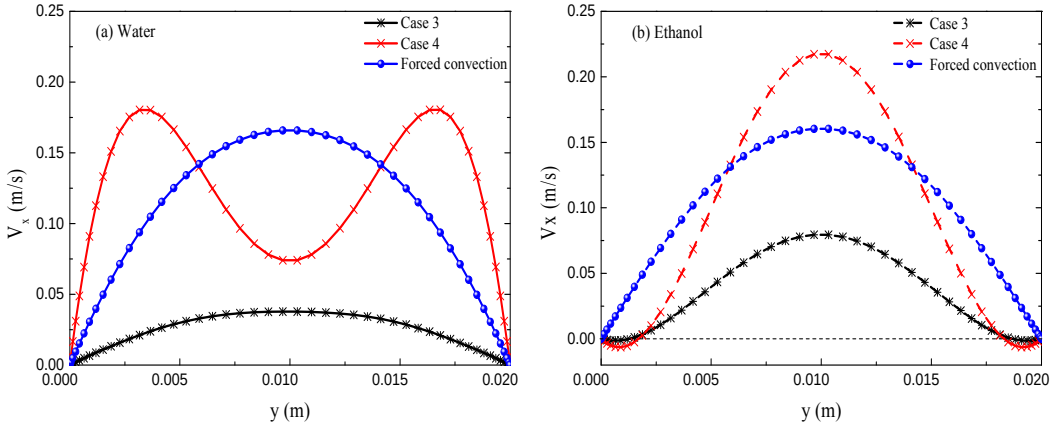

Fig. 5. Axial velocity profiles of water (a) and ethanol (b) at x = 0.1 m. Re_0 = 300, T_0 = 20 °C, ϕ_0 = 50°C.

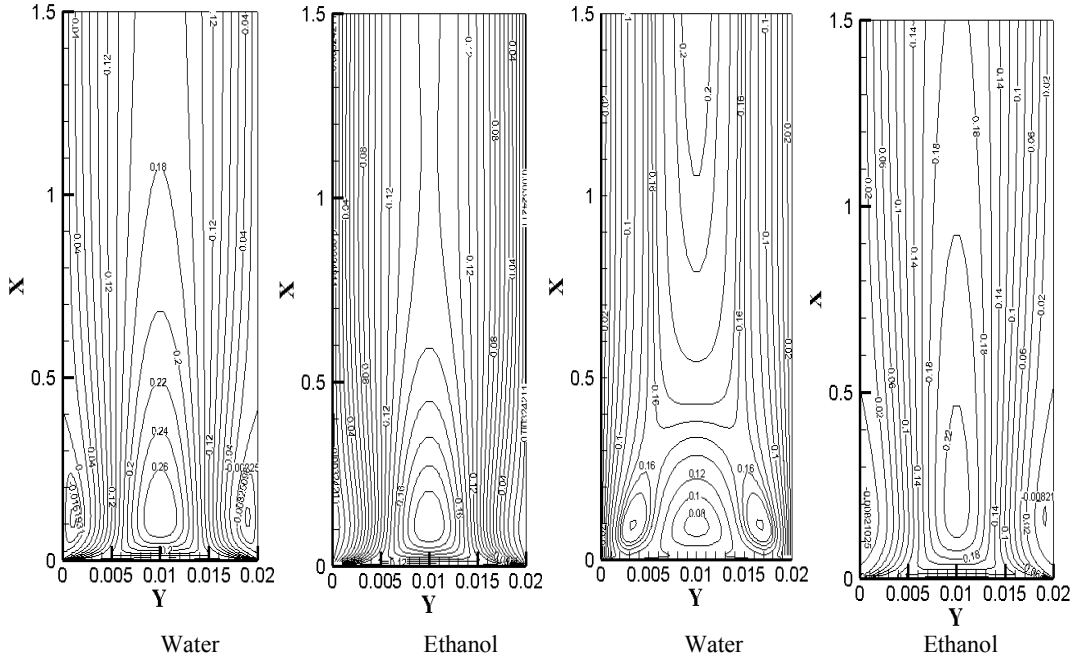

Fig. 6. Streamlines of axial velocity for cooling (a) and heating (b) modes of both mixtures.

inspection reveals that the air-ethanol mixture temperature profiles develop somewhat faster than those of air-water mixture, because the ethanol liquid film condenses more rapidly than water. The outcomes is a reduction of the average temperature of the flow until reaching the walls temperature T_w = 20 °C at the outlet of the channel. This trend is explained by the fact that the ethanol film has the lower latent heat of vaporization as depicted in Fig. 3(c). Note also that in the heating mode, air-water mixture presents more plated isotherms in the entrance region.

The axial evolution of the friction factors for the cooling and the heating mode is shown in Figs. 8 and 9, respectively, for the two liquid films. For comparison, the case of forced convection (Gr_T = Gr_M= 0) is also reported. We notice an important effect of buoyancy forces on this parameter in addition to the relative humidity of air at the entrance which is noticeable.

As seen from both figures, the axial evolution of the friction factor f_{Re} is monotonous in the case of forced convection and tends towards an asymptotic value at the channel exit. Indeed, we can distinguish that the values of the friction factor for both liquids are lower comparing to those of pure forced convection, except in case 4 for water, where the fiction factor is highest owing to the strong aiding buoyancy forces.

It is worth noting also that near the entrance of the channel, the friction factor f_{Re} decreases quickly and reaches its local minimum, which depends on the inlet air conditions. At this region, the intensity of the buoyancy forces is more important and the friction factor f_{Re} takes negative values in over some part of the channel. In those portions, the thermal and solutal buoyancy forces, opposed to the upward flow, overcome the forces of inertia ($|Ri^+| > 1$) and create a reversal flow by inducing a negative axial velocity and therefore, negative values of the friction factor f_{Re}. In case 4 for water, it is noted that the coefficient of friction f_{Re} decreases and reaches local minimums followed by local maximums near the entrance of the channel, due to the aiding thermosolutal

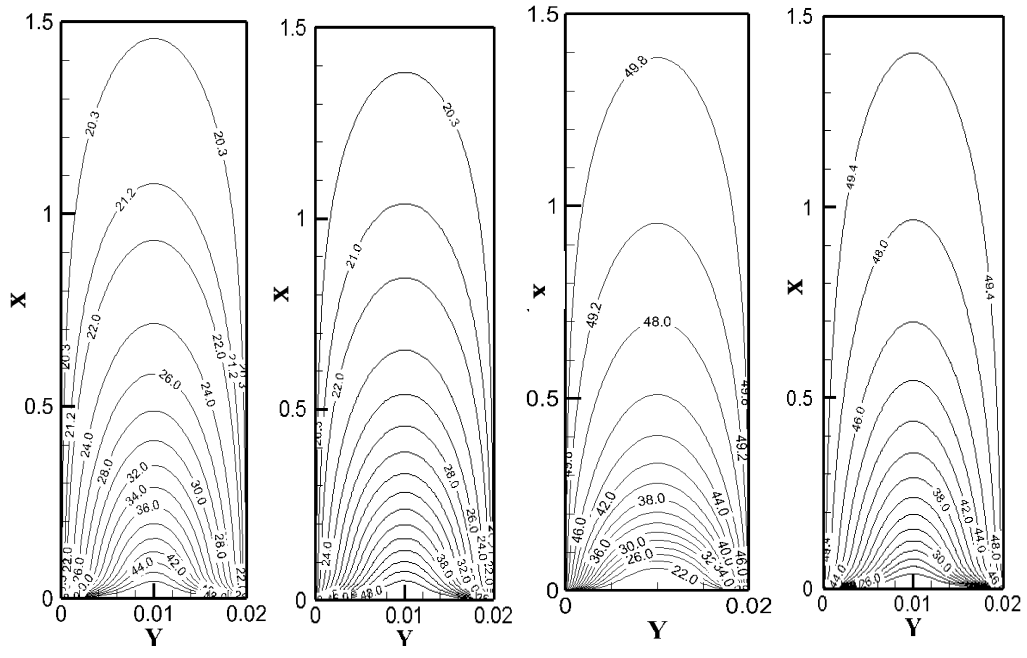

(a): Case 2 (b): Case 4

Fig. 7. Thermal fields in cooling (a) and heating (b) modes for both mixtures. Re_0 = 300.

buoyancy forces acting in the direction of flow ($Gr^+ > 0$). The aiding buoyancy forces accelerate the airflow near the channel walls. This results in an increase of the wall velocity gradient (Fig. 5(a)) and of the corresponding wall shear stress and friction factor. Beyond these positions, the buoyancy forces become weak comparing to the forces of inertia. The thermal and mass transfer between the wet plates and the flow is reduced as the flow goes upstream of the channel. Consequently, the friction factor f_{Re} for all cases tends towards the neighbours asymptotic value, 24, which is the analytical value for fully developed forced convection (Bejan 2004).

The mass transfer between the liquid film and airflow at the interface represented by the evaporation velocity (V_e) is shown in Figs.10 and 11 for the cooling and the heating modes, respectively.

In all the studied cases, the mass diffusion velocity takes large values near the entrance that the wall gradients of temperature and

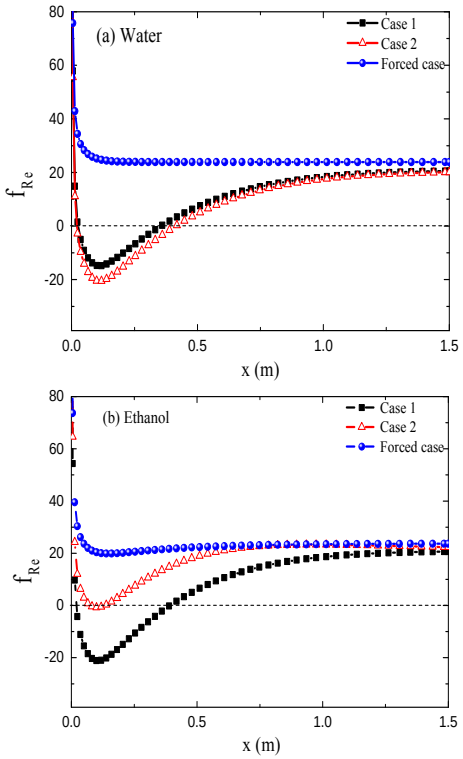

Fig. 8. Longitudinal evolution of the friction factor for water (a) and ethanol (b). Re_0 = 300, T_0 = 50°C, T_w = 20°C.

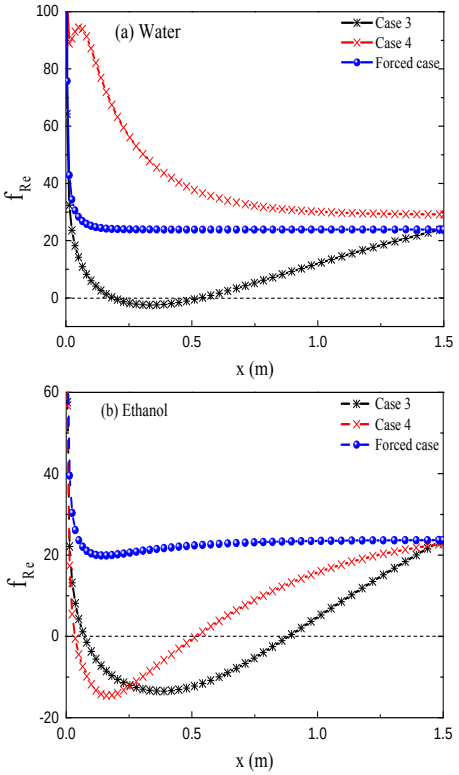

Fig. 9. Longitudinal evolution of the friction factor water and for ethanol. Re_0 = 300, T_0 = 20 °C, ϕ_0 = 50°C.

concentration are higher in this region. Gradually,as the air advances in the channel, it loses heat and moisture and therefore, the wall gradients of temperature and concentration decrease, which causes the decrease in the mass diffusion velocity. Therefore, the latter (V_e) tends monotonically towards zero. It is plausible to note that the positive values of the velocity tend to a liquid film evaporation (cases 3 and 4), whereas the negative values (case 2) indicate a condensation of the vapour on the walls. In case 1, there is no mass diffusion (V_e = 0) indicating that there is no phase change for this combination of variables, i.e.: $W_0 = W_w$.

It is also of interest to note that in all cases, the mass diffusion velocity tends toward zero at the exit of the channel, owing to the reduction of mass fraction difference as the flow goes upward.

The examination of these figures shows that there is a significant difference in mass diffusion velocity of water in comparison to ethanol.

In order to determinate precisely the conditions of existence of the flow reversal and its limits, a series of numerical simulations have been carried out in this section, investigating the effect of solutal buoyancy forces through the solutal Grashof number. Three values of the latter were considered: $Gr_M = -10^4$; 0 and -10^4. These series of numerical simulations allowed us to draw a map of flow reversal shown in Fig. 12.

We note from this figure that for a given solutal Grashof number Gr_M, the flow reversal curves are linear for both liquid films. Moreover, an increase of the Reynolds number increases the absolute thermal Grashof number which induces flow reversal, resulting of the increasing of the opposing thermal buoyancy forces.

The dependence of the thermal Grashof number on the Reynolds number is essentially linear and can be given by the following expressions for the water and ethanol films, derived from Fig. 12:

- **For air-Water mixture:**

$$Gr_T = 5826.26851 - 460.5639\ \mathrm{Re} \quad Gr_M = 10^4 \quad \text{(17-a)}$$

$$Gr_T = -4328.9256 - 460.63208\ Re \quad For \quad Gr_M = 0 \quad \text{(17-b)}$$

$$Gr_T = -13378.39325 - 458.53206\ Re \quad Gr_M = -10^4 \quad \text{(17-c)}$$

- **For air-Ethanol mixture:**

$$Gr_T = 12783.8289 - 558.89\,\mathrm{Re} \quad Gr_M = 10^4 \quad \text{(18-a)}$$

$$Gr_T = -5112.366 - 547.1289\ \mathrm{Re} \quad For \quad Gr_M = 0 \quad \text{(18-b)}$$

$$Gr_T = -15908.96193 - 549.03719\ \mathrm{Re} \quad Gr_M = -10^4 \quad \text{(18-c)}$$

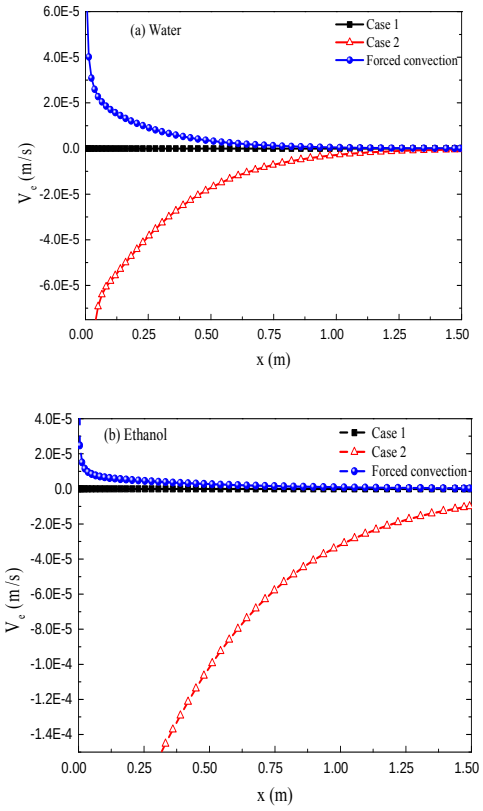

Fig. 10. Longitudinal evolution of the evaporation velocity for water and ethanol. Re_0 = 300, T_0 = 50°C, T_w = 20°C.

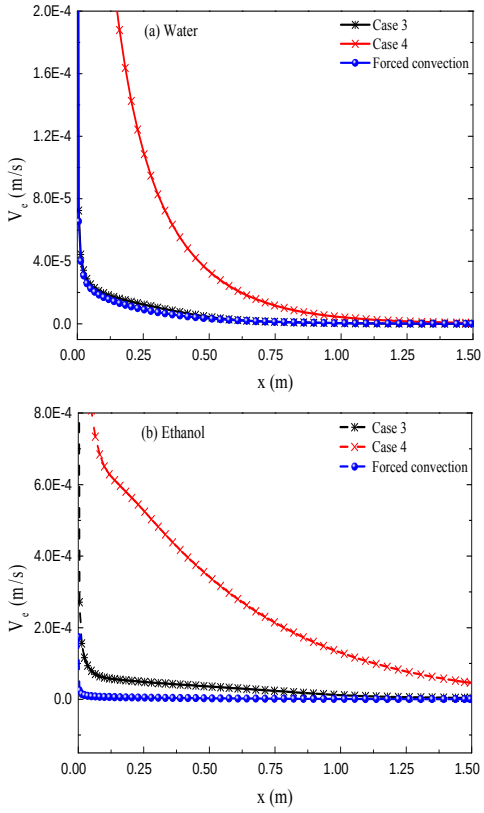

Fig.11. Longitudinal evolution of the evaporation velocity for ethanol. Re_0 = 300, T_0 = 20 °C, ϕ_0 = 50°C.

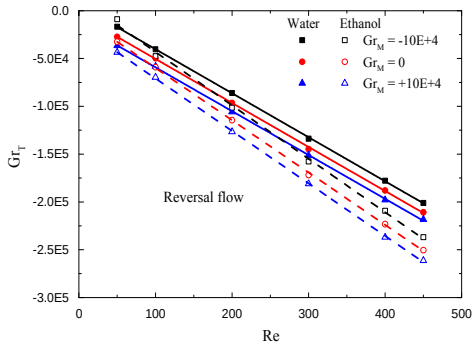

Fig. 12. Flow reversal chart.

5. CONCLUSION

The analysis carried out in this study has been developed to investigate numerically, using an elliptical flow model, the combining effect of thermal and mass buoyancy forces with evaporation or condensation of two different liquid films (water and ethanol), having widely different properties, for an upward laminar flow of humid air in a vertical parallel-plate with wetted walls. Various combinations of thermal and solutal boundary conditions (cooling and heating modes) are considered to investigate extensively their influence on the flow development for both liquids. Moreover, the conditions for the existence of flow reversal have been determined for different mass diffusion Grashof numbers of both systems.

Based to the obtained numerical results, the main conclusions are summarized as follows:

- The combining buoyancy forces, mostly of thermal origin, decelerate the flow of both liquid films near the walls and induce flow reversal for high temperature differences between the entrance gas mixture and the wet walls.
- Flow reversals are produced near the walls for both liquid films in the cooling case and for the ethanol film in the heating case.
- Flow reversal is more pronounced in the condensation case for the water film.
- The axial velocity profile is more distorted for high values of air humidity at the entrance for the water film unlike for the air-ethanol mixture, where the increase of humidity reduces the distortion of the axial velocity.
- The presence of the reversal flow perturbed the gas flow as well as the thermal field.

REFERENCES

Ait, H., Benhamou Z., Galanis B. (2004). Laminar mixed convection of humid air in a vertical channel with evaporation or condensation at the wall. *Int J thermal sciences* 43(6), 531-539.

Azizi, Y., Benhamou B., Galanis N., El-Ganaoui

M. (2007). Buoyancy effects on upward and downward laminar mixed convection heat and mass transfer in a vertical channel. Int J Num Meth Heat Fluid Flow 17(3), 333-353.

Bejan, A. (2004). Convection Heat Transfer, 4rd ed, Wiley & son.

Cherif, A. S., Kassim M. A., Benhamou B., Harmand S., Corriou J. P., Ben Jabrallah (2011). Experimental and numerical study of mixed convection heat and mass transfer in a vertical channel with film evaporation. *Int J Thermal Sciences* 50, 942-953.

Chien-Chang, H., W. M. Yan, J. Jer-Huan (2005). Laminar mixed convection heat and mass transfer in vertical rectangular ducts with film evaporation and condensation. *Int J Heat and Mass Transfer* 48, 1772-1784.

Chin-Heng, C., Hong-Sen K., W. H. Huang (1990). Flow reversal and heat of fully developed mixed convection in vertical channel. *J Thermophysics* 4(3), 375-383.

Debbissi, C., Orfi J., Ben Nasrallah S. (2003). Evaporation of water by free or mixed convection into humid air and superheated steam. *Int J Heat and Mass Transfer* 46, 4703-4715.

Desrayaud, G., Lauriat G. (2001). Heat and mass transfer analogy for condensation of humid air in a vertical channel. *J Heat and mass transfer* 37(1), 67-76.

Kassim, A., Benhamou B., Harmand S. (2011). Effect of air humidity at the entrance on heat and mass transfers in a humidifierintended for a desalination system. *Applied Thermal Engineering* 31, 1906-1914.

Lin, T. F., Chang C. J., Yan W. M. (1988). Analysis of combined buoyancy effects of thermal and mass diffusion on laminar forced convection heat transfer in a vertical tube. *J Heat Transfer* 110, 337-344.

Oubelle, M., Feddaoui M., Mir R. (2015). Numerical study of heat and mass transfer during evaporation of thin liquid film. *Thermal Science* 19(5), 1805-1819.

Oulaid, O., Benhamou B., Galanis N. (2012). Simultaneous Heat and Mass Transfer in Inclined Channel with Asymmetrical Conditions. *J Applied Fluid Mechanics* 5(3), 53-62.

Oulaid, O, Benhamou B, Galanis N (2010). Flow reversal in combined laminar mixed convection heat and mass transfer with phase change in a vertical channel. *Int J Heat and Fluid Flow* 31, 711-721.

Patankar, S. V. (1980). *Numerical heat transfer and fluid flow*, Hemisphere.

Perry, D. (1999) Perry's, *Chemical Engineers' Handbook*, Mc Graw-Hill, New York.

Reid, R. C., Praussita J. M., Sherwood T. K. (1977). *The properties of gas and Liquid, Hemisphere*, McGraw-Hill, New York.

Salah, El-Din M. M. (1992). Fully developed forced convection in vertical channel with combined buoyancy forces. *Int Commun Heat Mass Transfer* 19, 239-248.

Wang, M., Tsuji T., Nagano Y. (1994). Mixed convection with flow reversal in the thermal entrance region of horizontal and vertical pipes. *Int J Heat Mass Transfer* 37(15), 2305-2319.

Yan, W. M., Tsay Y. L., and Lin T. F. (1989). Simultaneous heat and mass transfer in laminar mixed convection flows between vertical parallel plates with asymmetric heating. *Int J Heat and Fluid Flow* 10(3), 262-269.

Yan, W. M., Lin T. F. (1988). Effect of wetted wall on laminar mixed convection in a vertical channel. *J Thermo Heat Transfer* 3, 94-96.